

A reflection-mode apertureless scanning near-field optical microscope developed from a commercial scanning probe microscope

G. Wurtz, R. Bachelot,^{a)} and P. Royer

Laboratoire de Nanotechnologie et d'Instrumentation Optique, Université de Technologie de Troyes, 12 rue Marie Curie, BP 2060, 10010 Troyes Cedex, France

(Received 30 June 1997; accepted for publication 20 January 1998)

We have developed a polyvalent reflection-mode apertureless scanning near-field optical microscope (SNOM) from a commercial scanning probe microscope (SPM). After having explained our motivations, we describe the instrument precisely, by specifying how we have integrated optical elements to the initial SPM, by taking advantage of its characteristics, and without modifying its initial functions. The instrument allows five different reflection-mode SNOM configurations and enables polarization studies. Three types of SNOM probes can be used: dielectric, semiconducting, and metallic probes. The latter are homemade probes whose successful use, as probes for atomic force microscopy, by the commercial SPM has been experimentally demonstrated. Using silicon–nitride (dielectric) probes, one of the five configurations has been experimentally tested with two samples. The first sample is made of nanometric aluminum dots on a glass substrate and the second sample is the output front facet of a laser diode. The preliminary SNOM images of the latter reveal pure optical contrasts. © 1998 American Institute of Physics. [S0034-6748(98)03404-2]

I. INTRODUCTION

Scanning near-field optical microscopy (SNOM)¹ has indisputably demonstrated its capability of achieving a sub-wavelength spatial optical resolution. Presently, this resolution is in the $[\lambda/10-\lambda/30]$ range, where λ is the wavelength of light. Nowadays, it is possible to consider two main SNOM families. The first one is the ‘‘aperture SNOM’’ which has given rise to most of the publications during the last decade. In its principle, this family uses a probe with a small aperture (diameter ~ 50 nm $\ll \lambda$) in a metallic screen placed at a small distance ($\ll \lambda$) from the sample surface to illuminate the sample locally (illumination mode²) or to pick up the optical near-field (collection mode³). This principle, which was suggested by Syngé⁴ and for the first time applied experimentally to optical wavelengths by Pohl *et al.*,² can be described by the Bethe–Bouwkamp theory.⁵ In general, SNOM apertures are produced from silica optical fibers or glass micropipettes. Despite its performances, aperture SNOM seems to have three limitations:

- (i) the optical resolution does not surpass 20 nm ($\sim \lambda/30$) which would correspond to the skin depth of the metal surrounding the aperture;
- (ii) making ultrasmall apertures is a technological challenge which presently prevents the mass production of such optical probes;
- (iii) aperture SNOM is limited to visible and near-infrared region of the spectrum. Indeed, it seems difficult to extend it to the mid- and the far infrared region because of the strong attenuation of the light power

transmitted by the silica fibers and the severe cutoff problem for metallized waveguides.

Additionally, the presence of the metallic screen (diameter > 100 nm) surrounding the aperture can generate feedback artifacts⁶ (in the case of an atomic force microscopy AFM/SNOM combination), and limits the study to samples without rough topographical structures.

The second family is the ‘‘apertureless SNOM’’ which uses apertureless tips as optical probes.^{7–12} In this case, the tip end may be viewed as some dipoles which, interacting locally with the sample surface, are excited by the optical near-field of the sample and radiate homogeneous waves which can be detected far from the sample surface. The resulting signal depends on the local optical properties of the sample just beneath the tip end. Hence, the tip end may be considered as a scattering Rayleigh particle, and this principle can be described by the Mie–Rayleigh theory.¹³ *A priori*, the refractive index n of the Rayleigh particle is complex ($n = n_1 + jn_2$). It can be noted that the scanning tunneling optical microscopy [(STOM),¹⁴ also called (PSTM)¹⁵ for photon scanning tunneling microscopy], may be considered as an ‘‘apertureless’’ SNOM using a dielectric ($n_2 = 0$) scattering particle, provided, of course, that an uncoated (non-metallized) probe¹⁶ is used. The apertureless SNOM family is less well known and much less used than the aperture SNOM. It arouses a growing interest, however, especially since it has demonstrated an 0.8 nm optical resolution,¹⁷ as well as its ability to work with a wavelength range much larger than that allowed by aperture SNOM.^{18–20} Another advantage is that the already existing AFM and STM (scanning tunneling microscopy) reliable probes can easily be used by apertureless SNOM.

Near-field optics is still a young branch of optics and it seems difficult to consider that the SNOM is already a ‘‘rou-

^{a)} Author to whom correspondence should be addressed; electronic mail: renaud.bachelot@univ-troyes.fr

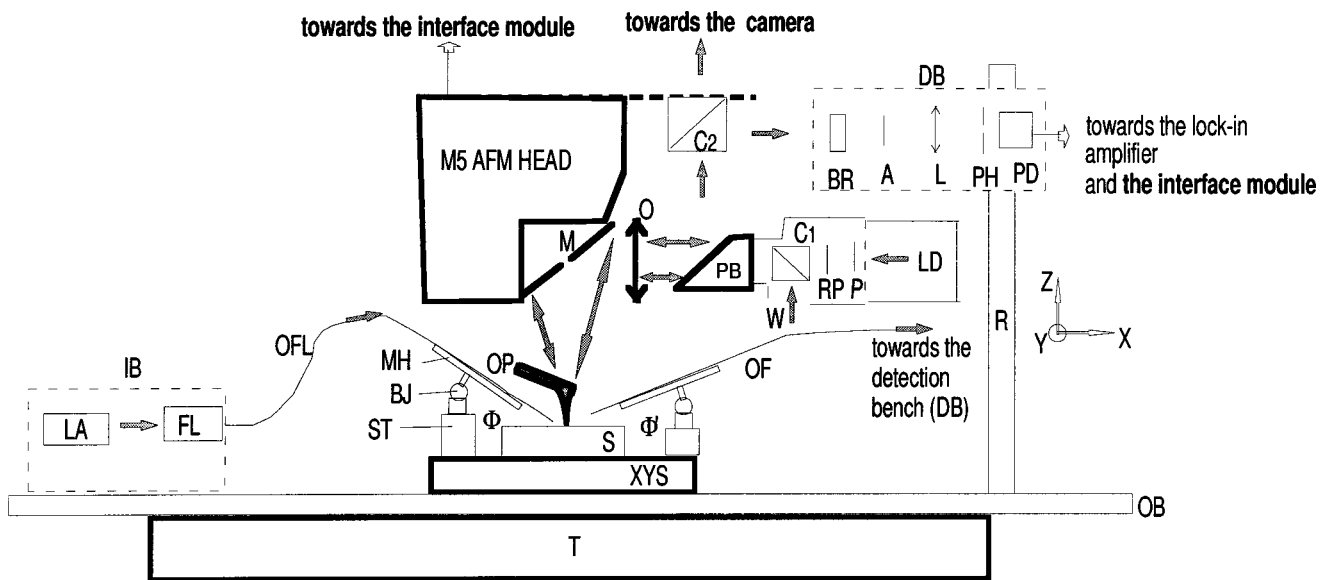


FIG. 1. General diagram of the main setup. The thick lines correspond to the initial commercial system. The thin lines represent the optical functions that we have integrated. The gray arrows represent the direction of light propagation. (A) analyzer, (BJ) ball joint, (BR) optical band rejector ($\lambda = 670$ nm) filter, ($C_{1,2}$) cube beamsplitters, (DB) detection optical bench, (FL) fiber launching (objective lens+positioner), (IB) illumination optical bench, (L) glass lens ($f = 100$ mm), (LA) laser source (He-Ne, Ar, laser diode...), (LD) laser diode ($\lambda = 635$ nm), with collimating optics and beam expander (X5), (M) pierced mirror, (MH) micro-pipette holder, (O) objective lens (X20, N.A.=0.28, W.D.=30 mm, $f = 10$ mm), (OB) optical breadboard, (OF) optical fiber ending in a micro-lens (N.A. ~ 0.5), (OP) cantilever and optical probe tip, (P) polarizer, (PB) piece holding a plate beamsplitter, (PD) photodetector, (PH) pinhole ($\varnothing = 40 \mu\text{m}$), (R) rod, (RP) retardation plate ($\lambda/2$ or $\lambda/4$), (S) sample, (ST) compact X,Y,Z translation stages, (T) active isolation tabletop, (W) white light, (XYS) sample chuck, XY translation stages, isolation rigid marble.

tine tool'' (like AFM and STM) for the study of local physical properties of samples. In fact, several fundamental problems have still to be solved. For example, the recent ''APPEAL'' of Hecht *et al.*⁶ is significant and leads us to question ourselves about the nature of the SNOM response and the respective influences of the topographical and dielectric local properties of the sample on the SNOM signal.

We have developed an apertureless SNOM from a commercial scanning probe microscope. The commercial SPM has been modified and has acquired an additional SNOM function. These modifications do not perturb the initial functions and performances of the SPM. Our motivations and expectations for such a development are the following:

- (i) to let the SNOM take full advantage of the capabilities and high quality of the commercial SPM system, including reliability, user-friendliness, reproducibility, stability, low noise electronics, data acquisition and processing, high quality piezo-transducers, available interface, and software;
- (ii) to use the various types of SPM probes as optical probes; and
- (iii) to easily combine and compare STM, AFM, SNOM techniques with each other.

With this setup, we hope to study and use the promising concept of ''apertureless SNOM'' under the best technological conditions. In this article, we describe the instrument in detail and present preliminary results and applications.

II. DESCRIPTION OF THE SETUP

During the description of the device, we will attempt to demonstrate its advantages by referring to the near-field op-

tics (NFO) literature. The modified commercial SPM is the M5 model from Park Scientific Instrument (PSI). This choice has been made according to several criteria. First, the system has an initial adjustable optics (objective lens, camera etc). Second, its mechanical environment is open enough to have access to the tip end (for illumination and detection of light). Third, the system is polyvalent: it permits AFM (contact, noncontact, or tapping modes) procedures, as well as lateral force microscopy (LFM), scanning tunneling microscopy (STM), and magnetic force microscopy (MFM).

A. General description

Figure 1 presents the general setup. We will see that this setup allows four SNOM configurations. On the other hand, we will see in paragraph II B that an auxiliary setup (that will be briefly described) allows a fifth configuration. The setup of Fig. 1 is the main device which takes advantage of the whole M5 environment, whereas the auxiliary system has been built outside this environment. In Fig. 1, the initial parts (of the commercial device) and the added elements are represented by thick lines and thin lines, respectively. Two main functions have been added, with regard to the initial system: an illumination function to illuminate the tip end by a focused laser beam, and a detection function to detect the scattered flux and to generate the SNOM signal.

1. Illumination of the tip end

Two illumination modes are possible: an illumination by a laser diode beam through a microscope objective and an illumination by an optical fiber terminating microlens.

Illumination by a laser diode beam through an objective lens (LD,P,RP,C1,PB,O,M, in Fig. 1). This illumination mode is compact and takes advantage of the initial optical

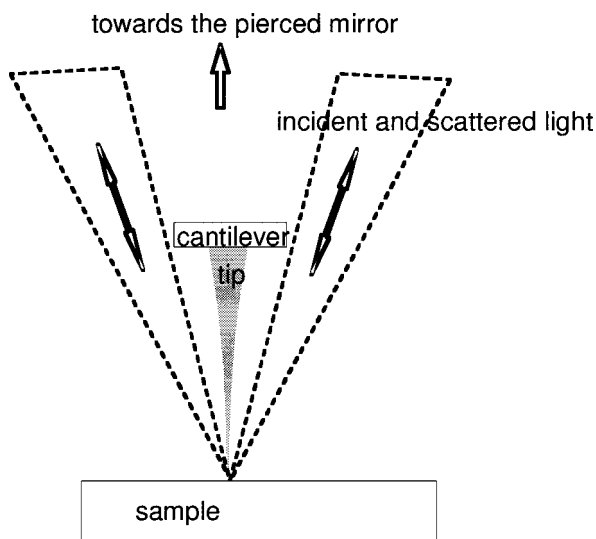


FIG. 2. Advantage of a dark-field illumination: the illumination of both the cantilever and the parts of the tip other than the extreme end is minimized. The axis of the cantilever is perpendicular to the page plane.

elements (PB,O,M in Fig. 1) used for visual observation of the sample surface. PB is initially an aluminum piece which holds a plate beamsplitter as well as a white light source. This source has been removed and replaced with the compact illumination system (LD,P,RP,C1 in Fig. 1). The use of this white light (W), however, is allowed by the cube beamsplitter C1, permitting the visual observation of the working field (sample, tip, and laser spots). A laser diode (LD, $\lambda = 635$ nm) has been associated with a beam expander ($\times 5$) providing a 10 mm diameter collimated laser beam. This diameter is necessary to illuminate entirely the entrance pupil of the objective lens (O, entrance pupil diameter=6 mm). Any kind of polarization state of this incident laser beam is allowed by both the polarizer (P) and the retardation plate (RP: $\lambda/2$ or $\lambda/4$).

This capability is of importance for a systematic study of polarization contrasts which are very significant in near-field optics. Although this study has often been made in aperture SNOM,^{21–23} it seems to be almost ignored in apertureless SNOM.²⁴ The objective lens (O) (infinity corrected, N.A. = 0.28) permits the focusing of the laser beam onto the sample surface. Since all of the entrance circular pupil of the objective is illuminated, the focalization spot is a diffraction spot whose diameter is $\sim 3 \mu\text{m}$ ($1.22\lambda/\text{N.A.}$). It has been shown that such a high density incident energy can be very effective in apertureless SNOM.^{10–12} The focused beam is deflected towards the sample by the mirror (M) which is initially pierced so that the laser beam ($\lambda = 670$ nm) issued from the M5 head can reach the cantilever (this laser beam, not represented in Fig. 1, permits by reflection the detection of the cantilever deflection). We noted that this hole does not prevent the generation of the diffraction spot on the sample surface. Moreover, the hole allows a “dark field” illumination which minimizes the illumination of both the cantilever and the parts of the tip other than the extreme end (Fig. 2). This illumination would generate a background optical signal which is unwanted because it is associated with a low spatial resolution.

In Fig. 1, it can be noted that the small size (compared to other laser sources) of the laser diode associated with the expander (about 3.5 cm diameter and 8 cm length) enables its total integration into the commercial system. This integration especially enables the Z movement of the laser spot by the focus M5 function which moves the compact set (O, PB, C1, RP, P, LD) in the X direction, as well as the X, Y movement of the spot, by the initial Z, Y adjustments of the microscope objective. All these possible adjustments are independent of the tip and sample positions.

Illumination by an optical fiber (OFL in Fig. 1). This illumination mode presents three advantages compared to the illumination by the objective. First, it allows one to use several types of laser source (LA in Fig. 1). Consequently, several wavelengths, light powers, and degrees of coherence can be tested. Second, it permits an oblique illumination. The angle Φ between the fiber axis and the sample surface can be adjusted in the 5° – 85° range. The influence of the angle of incidence on the near-field effect induced by the tip can thus be studied. This parameter Φ is of importance in apertureless SNOM. For example, in the case of strong enhancement of the electric field just below the tip,²⁵ it has been shown that the total field intensity beneath the tip apex strongly depends on Φ .²⁵ Third, in this case, we can be sure that the “dark-field” illumination is optimized: the incident light field illuminates neither the cantilever nor the parts of the tip other than its extreme end.

In Fig. 1, OFL is a single-mode optical fiber tapered by pulling under an electric arc. During the preparation of the taper, when the fiber breaks, the superficial tension leads to the formation of a microlens, whose radius of curvature and focal length are a few microns and a few tens of microns, respectively. This process ensures an adiabatic transition from the guided fundamental mode of the fiber to the extremity of the taper.²⁶ By optical measurements, we showed that such a system focuses the light to a $2 \mu\text{m}$ diameter spot, with a high (~ 0.5) numerical aperture. It is thus equivalent to a high power objective lens of micronic size. Such a fiber ending in a microlens has been successfully used as a probe for an optical profilometer.²⁷ The optical fiber (OFL) is held by a commercial pipette holder (H-7 Narishige, MH in Fig. 1), associated with a joint ball (B-8C Narishige, BJ in Fig. 1) and a XYZ translation stage (ST in Fig. 1). The compact system (MH, BJ, ST) permits the positioning of the laser spot on the sample surface as well as the adjustment of the angle Φ . The control of the polarization state is still possible with this illumination mode. Indeed, any desired polarization state is accessible for such a single-mode optical fiber which has already been successfully used for polarization studies.²¹

2. Detection of the SNOM signal

Two detection modes are possible: a detection by the objective lens, as well as a detection by an optical fiber.

Detection by the objective lens (M, O, PB, C2, DB in Fig. 1). In this detection mode, the objective lens (O, in Fig. 1) is used to collect the flux scattered by the SNOM probe in local interaction with the sample surface. The collimated laser beam issued from the objective lens is deflected first by

the initial plate beamsplitter (PB) towards the camera, then by the cube beamsplitter (C2, in Fig. 1) towards the detection bench. This added cube has simply been stuck on the input glass window of the camera, using an optical gel (refractive index = 1.46) which does not prevent optical observation and allows easy removal or adjustment of the cube. The detection bench (DB in Fig. 1) is a rail holding optical components. BR is a band rejector which rejects the wavelength of the laser beam ($\lambda = 670$ nm) issued from the M5 head, without cutting of that associated with the SNOM signal ($\lambda = 635$ nm). Indeed, light at $\lambda = 670$ nm would be unwanted background light scattered by the cantilever, mainly. The analyzer (A) is used in the case of polarization study. The light is focused by a lens (L) onto a pinhole (PH) and detected by a photodetector (PD). The spatial filter (PH) is used to reject the background scattered light: its diameter ($= 40 \mu\text{m}$) has been adjusted so that only the image of the diffraction spot, associated with the microscope objective, is detected.

Detection by an optical fiber (OF in Fig. 1). In this detection mode, the light scattered by the tip end is collected by an optical fiber (OF in Fig. 1) which is held by a mechanical system identical to that holding the fiber used for illumination. Hence, this mode permits an oblique detection with an adjustable angle of collection Φ' . This capability is of importance in near-field optics because the light emitted in different directions certainly has different behaviors and contains different information about the sample. For comparison, in the case of the "tunnel SNOM",²⁸ it has been recently shown that radiation emitted into directions within the critical angle of total internal reflection ("allowed light") contains information which is different and complementary to that contained by light emitted at supercritical angles ("forbidden light").²⁹ It is thus important to detect these two types of light, both of them but separately. Whatever the detection mode, the electric signal provided by the photodetector is processed by a lock-in amplifier at the vibration frequency of the AFM cantilever. We shall now show that it is necessary to use a vibrating AFM mode for an SNOM image generation.

3. Suitable AFM modes, lock-in detection, and scanning modes

In apertureless SNOM, because of the external illumination and detection, it is necessary to make the probe vibrate (perpendicular to the sample surface, at the frequency f) and to perform a lock-in detection (at the frequency f) of the scattered light. This procedure allows one to extract, from the total intensity received by the detector, the small part which corresponds to the light scattered by the local interaction between the tip end, the sample and the incident laser beam. Two suitable AFM modes are thus used: the "noncontact" mode^{10,17} and the "tapping mode" (or "intermittent contact" mode).^{11,12} These two modes are available on the M5 head. It has also been suggested to make both the tip (at f_t frequency) and the sample vibrate (parallel to its surface, at f_s frequency) and to detect the signal at the difference frequency $f_t - f_s$ (or at the sum frequency $f_t + f_s$).⁷ We will test this technique by installing the sample on a vibrating

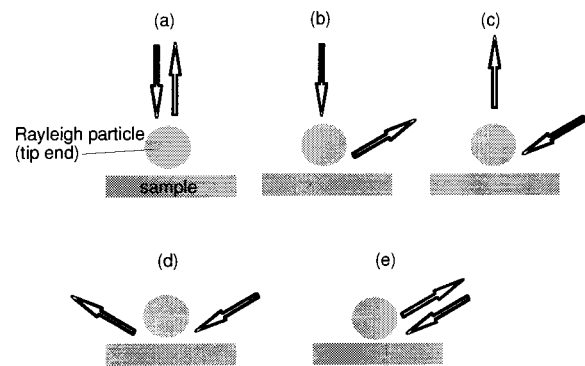


FIG. 3. Reflection-mode SNOM configurations allowed by our instrument. The sphere represents the tip end (Rayleigh particle). The arrows represent the direction of both incident and detected lights: (a) illumination by an objective, collection by an objective, (b) illumination by an objective, oblique collection by an optical fiber, (c) oblique illumination by an optical fiber ending in a micro-lens, collection by an objective, (d) oblique illumination by an optical fiber ending in a micro-lens, oblique collection by an optical fiber, (e) "backscattering" SNOM configuration allowed by the auxiliary setup presented in Fig. 4: both illumination and collection by an objective.

piezo-electric transducer. The lock-in amplifier that we use (EG&G Princeton applied research, 5302) is able to work in the 1 Hz–1 MHz range and is thus suitable for any resonance frequency of the AFM cantilevers.

In the case of the AFM/SNOM combination, two scanning modes can be used: the constant gap-width mode (CGM) and the constant height mode (CHM). CHM prevents feedback-induced artifacts^{6,30} in the SNOM image, but does not permit a very high resolution because the probe is not maintained in contact with the sample. Moreover, during scanning, the gap width (between the probe and the sample) is not constant in CHM, and therefore the optical resolution is also not constant because this resolution is very dependent on the gap width. CGM optimizes the SNOM resolution and simultaneously measures the topography. Nevertheless, this mode can generate serious artifacts in the SNOM image.^{6,30} When studying a sample, it is thus necessary to perform both CHM and CGM experiments, in order to obtain complementary images of the sample. The M5 head allows one to use these two scanning modes.

To finish this general description, it should be pointed out that both the M5 interface module and the user-friendly software allow the recording of several signals simultaneously, including the AFM signal, the corresponding error signal, and the SNOM signal (provided by the lock-in amplifier: amplitude and phase).

B. SNOM configurations

All the illumination/detection combinations are possible: illumination by the objective+collection by the objective, illumination by the objective+collection by the optical fiber, illumination by the optical fiber+collection by the objective, illumination by the optical fiber+collection by the optical fiber. Figure 3 presents these four configurations [(a), (b), (c), (d), respectively]. The fifth SNOM configuration [(e) in Fig. 3] is obtained by an auxiliary setup that we have developed outside the M5 system. Figure 4 presents this auxiliary

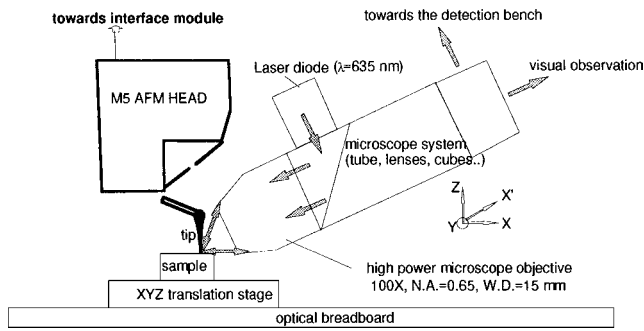


FIG. 4. Auxiliary setup allowing the “backscattering” apertureless SNOM configuration [(e) Fig. 3]. The X' axis is parallel to the microscope axis. The gray arrows represent the direction of the propagation of the light.

setup schematically. We take advantage of the fact that the M5 head can be removed and used out of the whole M5 system, above any sample, in a “stand-alone” configuration. This configuration is possible because in the M5 model the X, Y, Z piezoelectric scanner is integrated in the head associated with the probe. This removal frees a half-space near the tip, allowing the installation of an optical microscope system, associated with a high power microscope objective. This microscope system (objective+tube+lenses+cube beamsplitters+eye-piece) permits, simultaneously, the focusing of a laser diode beam ($\lambda = 635$ nm) onto the tip end, and the collecting of the “backscattered” light, and allows the user to observe the working field (laser spots, tip, and sample). With precision, the microscope system can be adjusted with regard to both tip and sample since it is held by a X, Y, Z, X' translation stages, and a rotation (around the Y, Z axis) stage (not represented in Fig. 4). A survey of the NFO literature reveals that this “backscattering” apertureless SNOM configuration has never been implemented.

C. SNOM probes

Three types of SNOM probes can be used: dielectric, semi-conducting, and metallic probes.

1. Dielectric probes

They are silicon-nitride (Si_3N_4 , refraction index ~ 2 at $\lambda = 635$ nm) commercial probes (Microlevers™ from PSI), the tip of which is pyramidal with a 70° vertex angle. The tip end is standard or sharpened. In the second case, the pyramid ends in a small 200 nm height tip, with a radius of less than 20 nm. Because of the low force constant of the cantilevers, these probes are suitable rather for contact-mode AFM. Nevertheless, the highest available force constant (0.5 N/m) allows one to perform both attractive mode and tapping-mode AFM procedures. This kind of pyramidal dielectric probe has been successfully used as SNOM probes.³¹ The preliminary images presented in this article have been obtained using such probes.

2. Semiconducting probes

They are boron-doped silicon (refraction index $\sim 3.8 + j0.02$ at $\lambda = 635$ nm) commercial probes (Ultralevers™ from PSI) with a conical tip. The typical radius of curvature for such a tip is less than 10 nm. The force constant of the cantilever are in the 0.2–20 N/m range, quite suitable for AFM vibrating modes. We also use tetrahedral silicon tips (micro-cantilever from Olympus). Such semiconducting tips have proven to be efficient as optical probes.^{10,17}

3. Metallic probes

The large interest of using metallic probes as SNOM probes has been theoretically^{25,32} and experimentally^{9,12} demonstrated. Nevertheless, no commercial metallic AFM probes exist. This is why we produce our own metallic tips. Moreover, this autonomy enables us to control the geometry of the tips which are made of tungsten. This material (W , $n \sim 3.7 + j2.8$, at $\lambda = 635$ nm) has proved to be efficient for SNOM probes.^{12,18,33} A tungsten cylindrical wire (diameter=125 μm) is polished and covered by a 100 nm thick gold layer, except at its extremity which is bent and etched by electrochemical erosion. This etching procedure is

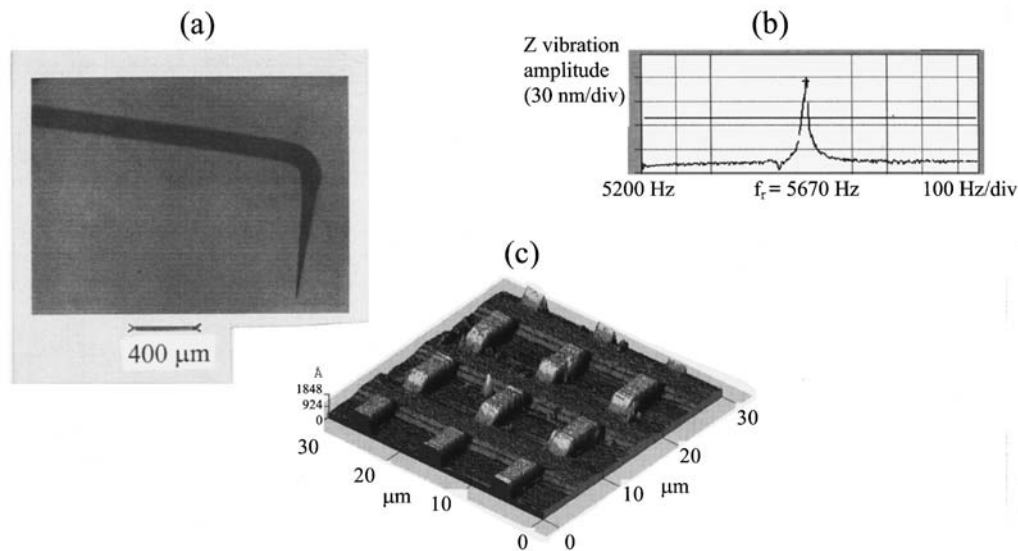


FIG. 5. Homemade tungsten (W) probes: successful use, as AFM probes, by the commercial SPM: (a) 2 mm×1.5 mm size snapshot of a W probe (cantilever and tip), (b) measurement of the resonance at frequency f_r , (c) 30 μm ×30 μm tapping-mode AFM image of a test grating.

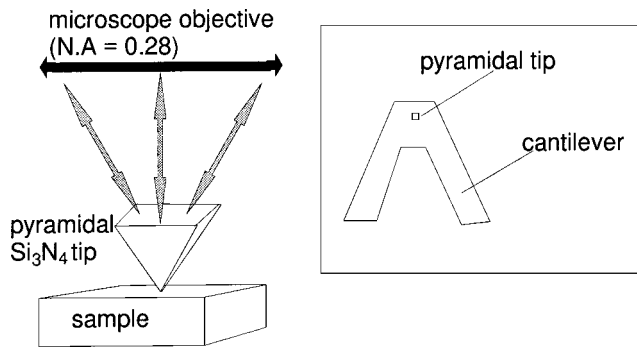


FIG. 6. Experimental configuration used to obtain the preliminary images: (Boxed) top view of the cantilever. The size of the pyramid base is $4\ \mu\text{m} \times 4\ \mu\text{m}$. The height of the pyramid is $4\ \mu\text{m}$. The gray arrows represent the direction of the propagation of the light.

described in several papers (e.g., Ref. 34). Figure 5(a) shows such a metallic probe. Both the well-tapered geometry of the tip as well as the large tip end-to-cantilever distance have to be noted. These characteristics are expected to minimize the unwanted background optical signal described above. The probe characteristics (length and shape of the tip, radius of curvature of the tip end) can be easily controlled by adjusting the parameters of the electrochemical procedure. The probes are checked by both conventional optical microscopy and scanning electron microscopy. The typical dimensions of the cantilever are $5\ \text{mm}$ (horizontal) by $0.5\ \text{mm}$ (vertical) and its stiffness constant k and resonant frequency f_r are in the $10\text{--}150\ \text{N/m}$ and $3\text{--}6\ \text{kHz}$ range, respectively. The cantilever is glued to a M5 ceramic cassette initially used to hold commercial cantilever chips. By choosing the glue point, the horizontal dimension of the cantilever is adjusted to choose both k and f_r . The radius of curvature of the end of such a homemade SNOM probe is less than $10\ \text{nm}$. Figures 5(b) and 5(c) demonstrate that these homemade probes can be used, as AFM probes, by the M5 system. The gold layer on the W cantilever, as well as the polishing, allows a reflectivity which is high enough for the laser beam ($\lambda = 670\ \text{nm}$) of the AFM head to permit the measurement of the vibration amplitude of the cantilever [as well as its resonance, Fig. 5(b)] and a tapping-mode AFM procedure [Fig. 5(c)].

Figure 5 presents preliminary experiments which show that we will be able to use metallic tips in the near future. Presently, this use is not optimized, notably because the initial electronic system of the SPM is not perfectly suitable for the low resonance frequency of the tungsten cantilever (typically $4\ \text{kHz}$). A small modification of this electronic system is in progress, in order to use the metallic tip as an optical probe under the best experimental conditions.

III. PRELIMINARY SNOM IMAGES

As mentioned in Sec. IV, this instrument will be used for the study of the apertureless scanning near-field optical microscopy. The preliminary images that we present here do not represent this study. The purpose of these images is to demonstrate that we have obtained a SNOM signal which

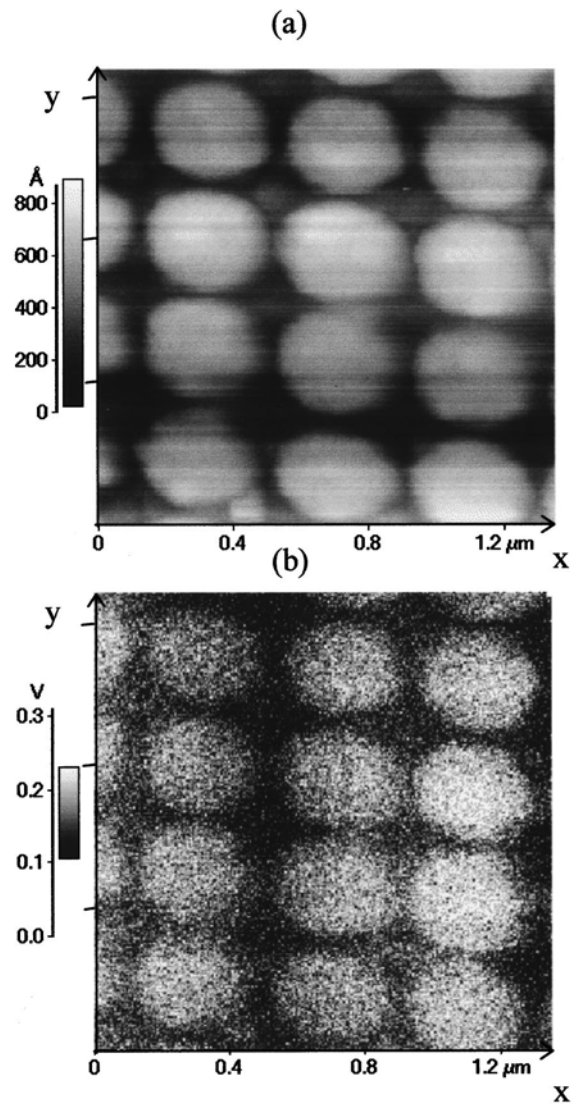


FIG. 7. Simultaneously obtained near-field images (size= $1.3\ \mu\text{m} \times 1.3\ \mu\text{m}$) of aluminum dots on a quartz substrate, obtained by the SNOM configuration of Fig. 3(a), with a silicon-nitride probe: (a) tapping-mode AFM image (constant-gap width mode, vibration amplitude $\sim 50\ \text{nm}$), (b) SNOM image (amplitude of the lock-in detection) at $\lambda = 635\ \text{nm}$.

seems to describe the subwavelength size optical characteristics of the sample. It should be pointed out that the following SNOM images are very reproducible.

The images have been obtained by implementing the (a) SNOM configuration [Fig. 3(a)], using a pyramidal silicon-nitride probe. The incident light ($\lambda = 635\ \text{nm}$) is focused by the objective, and the polarization contrasts are not taken into account (incident elliptic polarization, analyzer not used). Figure 6 describes the experimental conditions. Figure 7 presents the simultaneously recorded AFM image [tapping-mode, constant gap-width mode, vibration amplitude $\sim 50\ \text{nm}$, Fig. 7(a)], and SNOM image [amplitude of the lock-in detection, Fig. 7(b)] of aluminum patterns (dots) deposited on a quartz substrate. This sample has been prepared by x-ray lithography. The dots are $50\ \text{nm}$ high and are cylindrical (diameter= $200\ \text{nm}$) in shape and form a grating (period= $400\ \text{nm}$). Hence, this sample presents both known optical and topographical characteristics. In Fig. 7, we note

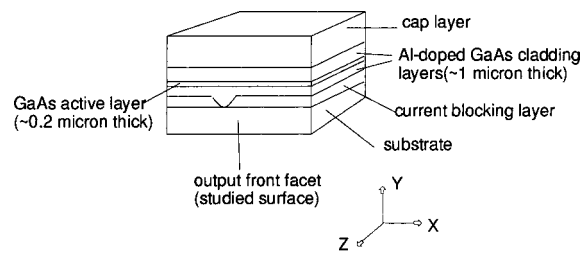


FIG. 8. Schematic diagram of the front facet of the laser diode used as sample. The Y axis is parallel to the growth direction. During near-field imaging, the axis of the probe tip is parallel to the Z axis, and the scan is in the (X, Y) plane.

that the resolution of the AFM images (better than 50 nm) seems to be slightly different from that of the SNOM image (about $50 \text{ nm} \sim \lambda/13$). For example, the two dots at the coordinates $(X=0.7 \mu\text{m}, Y=0.4 \mu\text{m})$ and $(X=1.1 \mu\text{m}, Y=0.4 \mu\text{m})$ are resolved in the AFM image, whereas they are barely resolved in the SNOM image. This difference between the AFM resolution and the SNOM resolution is not surprising because, *a priori*, the part of the tip in mechanical interaction with the sample surface does not exactly correspond to that in optical interaction with the sample. In the SNOM image [Fig. 7(b)], the observed contrast can be interpreted by the high optical reflectance of Al (at $\lambda=635 \text{ nm}$: reflectance $\sim 90\%$ at normal incidence, refraction index $\sim 1.3 + j7.5$), compared to that of quartz (reflectance $\sim 4\%$ at $\lambda=635 \text{ nm}$, at normal incidence). In any case the SNOM contrast has not been induced by a variation in the vibration amplitude, which has been kept constant by the AFM feedback (the error image, not presented in Fig. 7, does not present any contrast). In the AFM image, the presence of small particles lodged between Al dots can be noted, for example at the coordinates $(X=0.5 \mu\text{m}, Y=1 \mu\text{m})$. These objects are about 20 nm high. Although we are ignorant about their nature, we can assume that they are not Al particles because they do not correspond to any contrast in the SNOM image. For example, in the SNOM image, there is no distinguishable particle at the coordinates $(X=0.5 \mu\text{m}, Y=1 \mu\text{m})$. This leads us to hope for the independence of the SNOM signal and the local topography (and the AFM signal). Nevertheless, in the case of Fig. 7, topographical artifacts⁶ may be suspected. Indeed, since the configuration is in reflection, a spatial distribution of specular intensity $I_0(z)$ does exist. $I_0(z)$ is due to the interference between the incident light and the reflected light. Consequently, in this case the contrast of SNOM signal can depend on the path followed by the tip during the scan.³⁰ A good way to avoid this artifact is to study samples presenting no topographical contrast but a large optical contrast.²⁰ This is the case with the following sample.

Figure 8 presents a schematic representation of the sample studied next. It is the front facet of a commercial laser diode (GaAs/Al-doped GaAs, VSIS structure SHARP LT020MC, $\lambda=780 \text{ nm}$) whose protection window has been removed. The interest of this sample is that it does not present any topographic contrast (the crystal facet is cleaved) whereas it presents dielectric contrasts (various GaAs, GaAl_xAs layers). It is thus a suitable sample for first tests of

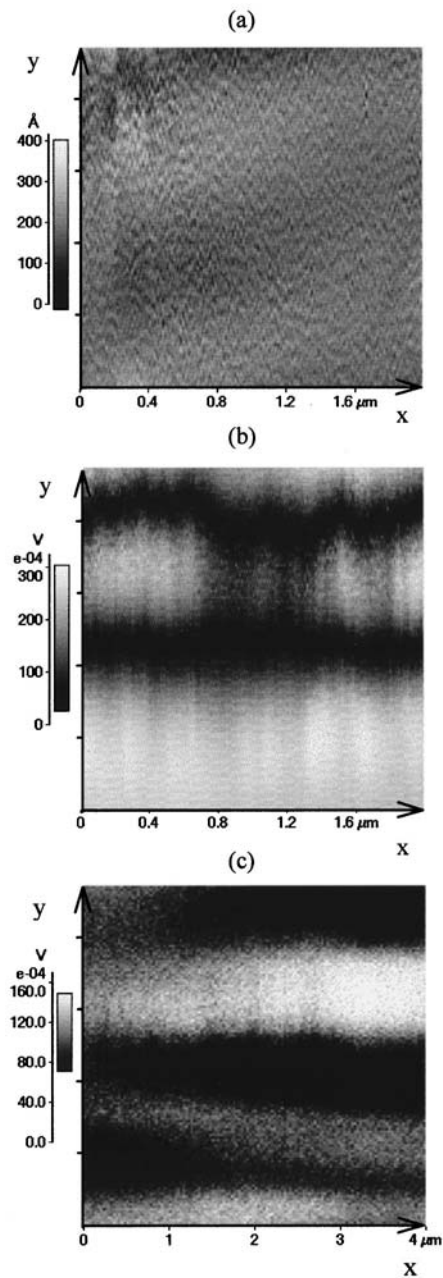


FIG. 9. Near-field images of the sample described in Fig. 8, obtained by the SNOM configuration of Fig. 3(a), with a silicon nitride probe: (a) $2 \mu\text{m} \times 2 \mu\text{m}$ size tapping-mode AFM image (constant-gap width mode, vibration amplitude $\sim 50 \text{ nm}$), (b) simultaneously obtained $2 \mu\text{m} \times 2 \mu\text{m}$ size SNOM image (amplitude of the lock-in detection) at $\lambda=635 \text{ nm}$, (c) $4 \mu\text{m} \times 4 \mu\text{m}$ size SNOM image of another sample zone.

the feasibility of our instrument. It should be noted, however, that the sample surface has certainly been covered by an antireflecting layer whose thickness is in the 10–100 nm range. Because of this layer, the microscope works in the “quasi-near field” zone.³⁵ In this zone, it has been demonstrated that a spatial resolution better than $\sim 100 \text{ nm}$ (at $\lambda=635 \text{ nm}$) cannot be reached.³⁵ Hence, we do not expect very high optical resolution with this sample. The images of Figs. 9(a) and 9(b) have been obtained in the same experimental conditions (see Fig. 6) as for Fig. 7. They are, respectively, the simultaneously recorded AFM (tapping mode, constant gap-width mode), and SNOM images of a sample

zone which is believed to include the active layer. For this experiment, the tip position above the sample was adjusted by visual observation of the spontaneous light emission from the active layer. Figure 9(a) shows the surface flatness. AFM quantitative measurements have confirmed that the surface roughness is less than 5 nm. It should be noted that this flatness corresponds to that of the antireflecting layer. The error image (not presented in Fig. 9) demonstrates that the tip vibration amplitude has been kept constant during scanning. The corresponding SNOM image [Fig. 9(b)] reveals various bands which are supposed to correspond to the GaAs/Al-doped GaAs layers of the laser diode structure. We interpret the contrast of this SNOM image by the fact that the refractive index of Al-doped GaAs is weaker than that of GaAs. It is presently difficult to identify the observed bands without both an advanced study of this sample and a better understanding of the imaging process in apertureless SNOM. However, it can be noted that the bands are parallel to the X axis, as expected (see Fig. 8). Moreover, it should be noted that if the sample is turned with an angle θ in its plane, then the observed band structure pivots in its plane with the same angle θ , demonstrating that the structure corresponds to the various dielectric layers parallel to the X axis. Figure 9(c) is a SNOM image of another zone of the sample. This image has been obtained using the same dielectric tip as for Fig. 9(b). In Fig. 9(c), six optical layers are distinguishable. As expected, in Figs. 9(b) and 9(c), the optical resolution is not very high compared to λ (~ 100 nm, i.e., $\sim \lambda/6$). However, this resolution represents a gain of about 30, compared to the resolution of the microscope objective used. In Fig. 9, no feedback artifact^{6,30} can be suspected in the SNOM images, and it is assumed that both Figs. 9(b) and 9(c) reveal a pure dielectric contrast. In Fig. 9, the size of the images do not exceed $4 \mu\text{m} \times 4 \mu\text{m}$. Larger scans would show the extended structure and would help to better identify the layers. Unfortunately, it is presently difficult to make a scan larger than about $4 \mu\text{m}$ because in our configuration both the laser spot (diameter $\sim 3 \mu\text{m}$) and the sample are fixed, whereas the probe is scanned above the sample. Hence, if the scan is too large, the probe leaves the spot and thus is no longer illuminated. This is a disadvantage as well as a limitation, which is why we actually install the sample on a piezoelectric transducer translation stage, for larger scans.

The SNOM characterization of this kind of sample (without an antireflecting layer to improve the resolution) is in progress. The light emission profile of the laser diode especially is studied for injection currents below as well as above the laser threshold.

IV. DISCUSSION AND PERSPECTIVES

In conclusion, we have presented a polyvalent reflection-mode apertureless SNOM developed from a commercial scanning probe microscope. The SNOM functions take advantage of the performances of the commercial system, without modifying them in any way. Two setups have been introduced, allowing five reflection-mode SNOM configurations which can use several types of tips of variable materials and shapes. One of the configurations has been

tested and the preliminary images have revealed the ability of the device to reveal the pure dielectric contrasts of a commercial optoelectronic component, with a subwavelength spatial resolution. Because of its polyvalence, this instrument is scheduled to allow the complete experimental study of the apertureless scanning near-field optical microscopy, including polarization contrasts, influence of the angle illumination, influence of the angle of detection, process of the SNOM signal formation, and influence of the tip nature (material and shape) on the SNOM contrast. Recent theoretical works³⁶ demonstrate that these experimental studies are of great importance. Simultaneously, the instrument will be used for characterization of components in microelectronics and optoelectronics, and for photopolymerization experiments. In this experiment, we will take advantage of the local extremely strong field enhancement that may occur in the gap between a metallic tip and a sample surface²⁵ to illuminate a sensitive sample locally, in order to perform optical lithography with a nanometric resolution.

ACKNOWLEDGMENTS

The authors are grateful to Y. Chen and R. Deturche for samples manufacture, M. Spajer and D. Courjon for microlens manufacture, P. Adam, O. Bergossi, J. L. Bijeon, R. Carminati, and J. J. Greffet for fruitful discussions, and A. C. Boccara for encouragement.

- ¹M. A. Paesler and P. J. Moyer, *Near-Field Optics* (Wiley, New York, 1996); J. P. Fillard, *Near-Field Optics and Nanoscopy* (World Scientific, Singapore, 1996).
- ²D. W. Pohl, W. Denk, and M. Lanz, *Appl. Phys. Lett.* **44**, 651 (1984).
- ³E. Betzig, M. Isaacson, and A. Lewis, *Appl. Phys. Lett.* **51**, 2088 (1987).
- ⁴E. H. Syngde, *Philos. Mag.* **6**, 356 (1928).
- ⁵H. A. Bethe, *Phys. Rev.* **66**, 163 (1944); C. J. Bouwkamp, *Phillips Res. Rep.* **5**, 401 (1950).
- ⁶B. Hecht, H. Bielefeld, Y. Inouye, and D. W. Pohl, *J. Appl. Phys.* **81**, 2492 (1997).
- ⁷A. C. Boccara, MRT Contract 88 PO249 (Ministère de la recherche et de la technologie, Paris, France, 1988); H. K. Wickramasinghe and C. C. Williams, U.S. Patent 4,947,034 (Aug. 28, 1990).
- ⁸R. Bachelot, P. Gleyzes, and A. C. Boccara, *Microsc. Microanal. Microstruct.* **5**, 389 (1994).
- ⁹Y. Inouye and S. Kawata, *Opt. Lett.* **19**, 159 (1994).
- ¹⁰F. Zenhausern, M. P. O'Boyle, and H. K. Wickramasinghe, *Science* **249**, 1083 (1995).
- ¹¹R. Bachelot, P. Gleyzes, and A. C. Boccara, *Opt. Lett.* **20**, 1994 (1995).
- ¹²R. Bachelot, P. Gleyzes, and A. C. Boccara, *Appl. Opt.* **36**, 2160 (1997).
- ¹³G. Mie, *Ann. Phys. (Leipzig)* **25**, 377 (1928); M. Born and E. Wolf, *Principles of Optics*, 6th ed. (Pergamon, New York, 1993), Chap. 13.5.
- ¹⁴D. Courjon, K. Sarayedine, and M. Spajer, *Opt. Commun.* **71**, 23 (1989).
- ¹⁵F. de Fornel, J. P. Goudonnet, L. Salomon, and E. Leniewska, *ECO2 Opt. Storage Scanning Technol.* **1139**, 77 (1989); R. C. Reddick, R. J. Wurmack, and T. L. Ferrel, *Phys. Rev. B* **39**, 767 (1989).
- ¹⁶C. Bainier, S. Leblanc, and D. Courjon, in *Near Fields Optics*, Vol. 242, *NATO ASI Series E: Applied Sciences*, edited by D. W. Pohl and D. Courjon (Kluwer, Dordrecht, 1993), p. 97.
- ¹⁷Y. Martin, F. Zenhausern, and H. K. Wickramasinghe, *Appl. Phys. Lett.* **68**, 2475 (1996).
- ¹⁸A. Lahrech, R. Bachelot, P. Gleyzes, and A. C. Boccara, *Opt. Lett.* **21**, 1315 (1996).
- ¹⁹B. Knoll, F. Keilmann, A. Kramer, and R. Guckenberger, *Appl. Phys. Lett.* **70**, 2667 (1997).
- ²⁰A. Lahrech, R. Bachelot, P. Gleyzes, and A. C. Boccara, *Appl. Phys. Lett.* **71**, 575 (1997).
- ²¹E. Betzig, J. K. Trautman, J. S. Weiner, T. D. Harris, and R. Wolfe, *Appl. Opt.* **31**, 4563 (1992).

- ²²K. Propstra and N. F. van Hulst, *J. Microsc.* **180**, 165 (1995).
- ²³A. Jalocha and N. F. van Hulst, *J. Opt. Soc. Am. B* **12**, 1577 (1995).
- ²⁴To our knowledge, only Adam *et al.* have recently begun this study: P. M. Adam, J. L. Bijeon, and P. Royer, Fourth International Conference in Near-Field Optics (NFO-4), Jerusalem, Israel, Feb. 9–13, 1997 (oral communication).
- ²⁵O. J. F. Martin and C. Girard, *Appl. Phys. Lett.* **70**, 705 (1997).
- ²⁶H. Kuwahara, M. Sasaki, and N. Tokoyo, *Appl. Opt.* **19**, 2578 (1980).
- ²⁷M. Spajer, O. Bergossi, and M. Guignard, *Opt. Commun.* **106**, 139 (1994).
- ²⁸B. Hecht, D. W. Pohl, and H. Heinzelmann, *Ultramicroscopy* **57**, 229 (1995).
- ²⁹L. Novotny, *J. Opt. Soc. Am. A* **14**, 91 (1997); *ibid.* **14**, 105 (1997).
- ³⁰R. Carminati, A. Madrazo, M. Nieto-Vesperinas, and J. J. Greffet, *J. Appl. Phys.* **82**, 501 (1997).
- ³¹N. F. van Hulst, M. H. P. Moers, O. F. J. Noordman, R. G. Tack, F. B. Segerink, and B. Bölger, *Appl. Phys. Lett.* **62**, 461 (1993); F. Baida, D. Courjon, and G. Tribillon, in *Near Field Optics*, Vol. 242, *NATO ASI Series E: Applied Sciences*, edited by D. W. Pohl and D. Courjon (Kluwer, Dordrecht, 1993), p. 71.
- ³²R. D. Grober, R. J. Schoelkopf, and D. E. Prober, *Appl. Phys. Lett.* **70**, 1354 (1997).
- ³³M. Specht, J. D. Pedarnig, W. M. Heckl, and T. W. Hansch, *Phys. Rev. Lett.* **68**, 476 (1992).
- ³⁴A. J. Melmed, *J. Vac. Sci. Technol. B* **9**, 601 (1991).
- ³⁵D. Barchiesi, O. Bergossi, C. Pieralli, and M. Spajer, *Ultramicroscopy* (to be published).
- ³⁶A. Madrazo, R. Carminati, M. Nieto-Vesperinas, and J. J. Greffet, *J. Opt. Soc. Am. A* **15**, 109 (1998).